TOWARD MAGMATIC SOURCE MODELS FOR NGAKURU GRABEN, TAUPO RIFT, NEW ZEALAND

Susan Ellis[1], Warwick Kissling[1], Andrew Rae[2] and Pilar Villamor[1]

[1]GNS Science, PO Box 30-368, Lower Hutt 5040, New Zealand

[2]GNS Science, 114 Karetoto Rd, Wairakei 3377, New Zealand

s.ellis@gns.cri.nz

Keywords: *magma, heat-flow, rift, graben. Ngakuru, Taupo Volcanic Zone*

ABSTRACT

A thermo-mechanical code is used to model heat transfer in the ductile region below the Taupo Rift constrained by crustal resistivities derived from MT measurements. We investigate how magmatic fluid and heat are transported to the upper, brittle crust and affected by underplating, fluid flux from the subduction system beneath the rift, and thinning of inherited basement in the rift. We show that intrusion and underplating of melt within and below the brittle crust are necessary to attain sufficient heat-flow at the base of the permeable brittle crust. These results are used to inform more detailed models of fluid flow through the Ngakuru graben fault system which aim to explain the presence of surface hydrothermal activity throughout this system during the last 30 kyr.

1. CONSTRAINING SOURCE MODELS FOR HEAT AND FLUIDS AT THE ROOT OF GEOTHERMAL SYSTEMS

1.1 Rationale for study

Ultimately, heat and geothermal fluid flow in the Taupo Volcanic Zone (TVZ) are driven by deep crustal magmatic intrusions derived from subduction of the Hikurangi slab and subducting sediments beneath the North Island. How heat and fluids transfer from deep to shallow levels determines the appropriate boundary conditions that should be used in shallow reservoir models. In particular, which boundary conditions are appropriate at reservoir scale when shallow melt is present within brittle crust (i.e. 4-8 km depth) and how should these boundary conditions change when melt is restricted to greater depths, i.e. beneath the brittle-ductile transition (BDT)? How does the observed average surface heat-flux of ~ 700 mWm^{-2} for the central TVZ (Bibby et al., 1995) relate to heat-flux at depth? Similarly, what are the implications of the high fluid flux rates estimated at the surface ($cmyr^{-1}$; Bibby et al., 1995; Sibson and Rowland, 2003) for fluid and magma entering the base of the crust?

Several useful studies have estimated the contribution of magma, fluids and other factors to surface heat flux in the TVZ (e.g., Bibby et al., 1995; Hochstein, 1995; Weir, 2003). Crustal geophysical measurements have also highlighted the critical role that structure plays in transporting heat and fluids to the surface (e.g., Bertrand et al., 2012; Bertrand et al., in press). Using coupled thermo-fluid-mechanical models we are attempting to refine heat transfer estimates in the crust in light of recent geophysical studies- in particular, to explore the effect of structure, faults as down-flow zones, and shallow magma sources on heat transfer. This paper is a progress report of models to-date, although we caution that results are so far preliminary and need further discussion and refinement.

Our models are based loosely on the Ngakuru graben in the central TVZ, which hosts a number of major geothermal areas on its western and eastern margins – including Te Kopia, Waikite, Orakeikorako, Atiamuri and Horohoro. As well as these active geothermal systems, areas of extinct hydrothermal activity (i.e. silica sinter, hydrothermal eruption deposits and hydrothermally-altered tephras and lake sediments) are also found at the margins of the graben, including its northern and southern terminations. The graben contains four major active faults (or fault systems) – the Ngakuru, Maleme, Whirinaki and Paeroa. These not only define the graben structurally but play host to its hydrological system which, because of the deep interconnectedness of the faults, can behave in a complex way when there are significant, sudden changes in the fault permeabilities. Such changes are expected to have implications for the location and longevity of past geothermal activity in the graben, as interpreted from fossil sinter formations and other manifestations (Kissling et al., 2015).

The deep magmatic roots of the central TVZ have been imaged using magnetotelluric (MT) electrical resistivity imaging (Heise et al., 2007; 2010). Resistivity less than 10 Ωm is generally interpreted to represent partial melt at depth, although at shallow levels of the crust (a few kms) such zones may indicate presence of fluids and clays rather than melt. Low-resistivity zones extend from below the brittle-ductile transition towards the base of the crust, underlying the rift axis (Heise et al., 2013). Geologically reasonable estimates of the melt fraction required to explain an observed resistivity are obtained by assuming that the basaltic melt is at a temperature between its solidus and liquidus. Since the resistivity of fully molten basalt is lower than 1 Ωm (e.g., Waff and Weill, 1975), if these are interpreted as an assemblage of intruded mafic sills or dikes, they suggest partial melt of < 20% (e.g., Rippe and Unsworth, 2010) or a complex superposition of solidified and underplated material. However, the inference of melt fraction from a resistivity measurement is ambiguous; there is a trade-off between melt fraction and temperature to explain a given resistivity.

MT inversions using data from a denser array of stations have allowed more detailed shallow imaging to a depth of 10 km of the southern part of the Ngakuru graben (Bertrand et al., 2012; in press). These studies show zones of low resistivity at ~3-6 km depth, interpreted as recent intrusions feeding heat and magmatic fluid to associated geothermal fields (e.g., Rotokawa, Ngatamariki and Ohaaki), while other geothermal fields do not appear to be underlain by shallow resistivity anomalies. Bertrand et al. (in press) suggest that there is an association between shallow intrusions and the margins of old caldera collapse structures, i.e. that geological structure and magmatic intrusions can in some cases play a direct role in feeding geothermal systems.

1.2 Models of heat and fluid transfer in the TVZ

1.2.1 1D models of heat transfer from underplating

The perturbation in heatflow as a function of depth can be calculated for each component of the system represented in Figure 1. For the calculations presented here we use the finite element code SULEC, which solves for thermo-mechanical evolution and has previously been used to study the interaction between rifting, melt and fluid flow in the TVZ (Ellis et al., 2014).

We demonstrate this first of all using simple one-dimensional models through the centre of the graben. The initial model (M1) represents only the effects of a basaltic layer underplating the crust at a constant rate for the past 1 My.

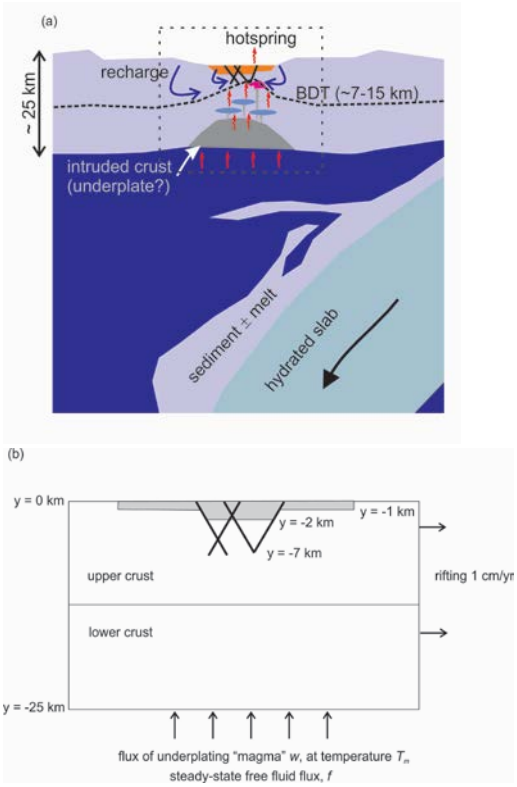

Figure 1: (a) Schematic illustration of heat transfer mechanisms and large-scale structure beneath the Ngakuru graben (not to scale; structure based on Harrison and White, 2006 and Stern et al., 2010). Red arrows indicate heat and fluid influx from below while blue arrows indicate fluid recharge and downwelling. BDT = depth of brittle-ductile transition, inferred from seismicity (b) Close-up of region in dotted boxed from a).

This simple 1D model is similar to earlier analytical solutions by Hochstein (1995); in fact we first tested our numerical code by reproducing Hochstein's results, although those shown in Figure 2 (black lines) have been modified to take into account more recent estimates of melt fraction near the base of the crust based on typical resistivities there of 2-10 Ωm (Heise et al., 2007; 2010).

We start with a crustal thickness of 25 km and assume that 5 km of basaltic melt is underplated in 1 My, corresponding to an underplating rate of 5 mm yr^{-1}. This represents upwelling required to fill the space created by extension (at 1 $cmyr^{-1}$) of a 60-km-wide rift in 1 My, although we do not include extension in this 1D model. Assuming that, at steady-state, the rate of underplating is balanced by rate of solidification, this should contribute an additional heat-flux of ~ 130 mWm^{-2}.

We assume upper and lower crustal properties are the same, with a latent heat of fusion of 4×10^5 J kg^{-1}, a density of 2800 kg m^{-3} and thermal conductivity 2.8 W $m^{-1}K^{-1}$. We do not model faults or sediment. The flux of free fluid from the underlying subduction system is neglected. $T_{solidus}$ and $T_{liquidus}$ for greywacke are assumed to be 800°C and 915°C and melt fraction varies linearly with temperature between these limits (a simplified, linearised version of parameter values used in the models of Annen et al., 2005). For underplating basalt, we use a thermal conductivity of 3 W $m^{-1}K^{-1}$, $T_{solidus}$ = 900°C and $T_{liquidus}$ =1300°C and a latent heat of fusion of 3.2×10^5 J kg^{-1}.

We assume an initial geothermal gradient of 16 °C km^{-1}, corresponding to a background heat-flow of 45 mW m^{-2}. The top boundary has a temperature of 20°C, while the lower boundary has a prescribed underplated flux at a temperature of 1100 °C. This is below the liquidus, giving a partial melt fraction of 0.5 for hydrated (3.8 wt% water) basalt. This is probably still too high to reproduce typical resistivities measured near the base of the crust at 30 km depth (Heise et al., 2007; 2010).

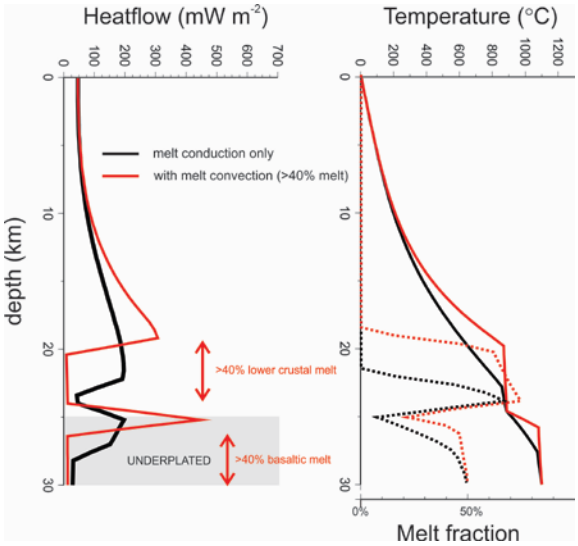

Figure 2: Heatflow (left), temperature profile (right) and melt fraction (right, dotted lines) for model M1 after 1 My of underplating (black). Grey shading shows final extent of underplated material. Red lines are a variant of M1 where melt convects for melt fractions greater than 40%.

Figure 2 shows the resultant melt fraction, heat-flow and temperature predicted by model M1 as a function of depth after 1 My (black lines). The underplated material at this time is shown by grey shading. A maximum melt fraction of 50% is present at the just-underplated base of the crust. Above the underplate layer, a second melt region is predicted (black dashed line) with up to 65% melt in modelled greywacke crust, which has a lower solidus temperature. This lower crustal melt forms as a result of temperatures conducting away from the underplated basaltic layer; note however that model M1 does not include melt advection, so melt forms and resides in situ. A peak heat-

flow of ~200 mWm^{-2} occurs just above the underplated layer and within the lower crustal melt region, falling away to typical base values of 40-50 mWm^{-2} at the surface. This model, as well as producing melt fractions in greywacke crust that are too high to be compatible with the MT inversions, is therefore unable to explain the elevated surface heat flow in the TVZ although heat flow is elevated at depth (see also Hochstein, 1995). An alternative model, where instead of sills, basaltic dikes are injected into the lower crust, was shown by Hochstein to similarly underestimate surface heat-flow. A slightly broader lower crustal thermal and heat-flow anomaly is produced when sills are assumed to be injected at random depths between the Moho and Conrad discontinuity in the crust (Annen et al., 2005).

A variation of model M1 is also shown on Figure 2 (red lines). In this model, it is assumed that at melt fractions of > 40%, melt can freely convect (e.g., Rosenberg and Handy, 2005). Such small-scale convection is represented by increasing melt conductivity by a factor of 10, thus producing almost isothermal regions where melt is present. This increases heatflow and the thermal anomaly in the lower crust (also the amount of lower crustal melt) but the basic conclusions remain the same.

The results of model M1 are not surprising since, clearly, more than conductive heat flow is required to transfer excess heat from depth to the surface in a magmatic rift. Additional advective heat transfer is required, for example by fluids and/or melt advection in the crust.

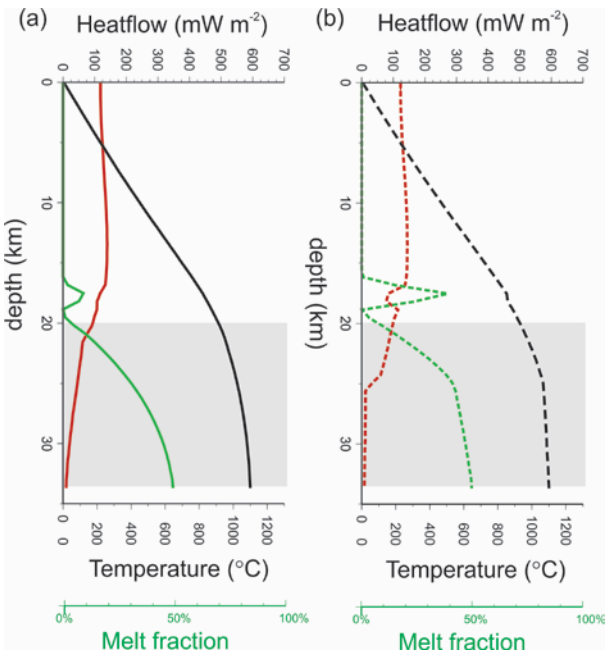

Figure 3: Results for model M2 after 3 My of underplating and stretching. (a) (solid lines) no melt convection; (b) (dashed lines) with melt convection for melt fraction > 40%. Black is temperature; red is heat-flow; green shows melt fraction. Grey shading indicates zone of underplated and stretched basalt.

1.2.2 1D models of heat transfer from underplating and rifting

An obvious criticism of the use of the Stefan problem-type boundary conditions (e.g., Hochstein, 1995; model M1) is that it does not take into account the thinning of the crust during underplating. In model M2, we repeat the underplating experiment but this time we assume an initial crustal thickness of 30 km. The underplating rate is taken as 6.6 $mmyr^{-1}$ to give a final crustal thickness of ca. 35 km after 3 My of stretching at an assumed stretching rate of 1 cm yr^{-1} over 60 km width; that is, the addition of material from underplating slightly exceeds the thinning owing to rifting and stretching of the crust. This creates maximum basaltic melt at a depth of 35 km, consistent with an observed bright-spot reflector seen at this depth by Stratford and Stern (2006). After 3 My the greywacke crust has been thinned to 20 km, i.e. a stretching factor of ~1.5 and is underlain by underplated (and also partially stretched) basalt 15 km thick (Figure 3).

The extra heat influx in the base of this model results from (1) a higher rate of underplating and (2) thinning of the crust and underplated material at a rate that brings hotter material closer to the surface, since conduction cannot keep pace with it. This leads to a maximum heat-flow of ~ 120 mW m^{-2} (Figure 3a), which occurs throughout the felsic crust, suggesting that the effect of thinning dominates the heat-flow. Only a small percentage of melt is generated in the greywacke layer (<10% for the model with no melt convection (Figure 3a), with a total thickness of a few km). The thicker underplate layer thermally insulates the crust from higher temperatures.

1.2.3 1D models of heat transfer from underplating, rifting and fluid flux

Estimates of total fluid produced at depth by slab dehydration using thermal subduction models (e.g., van Keken et al., 2011) yield average fluid flow of about 0.5-2 mm yr^{-1} averaged over a 60-km-wide rift. Most of this fluid will be transported in hydrated melt to the base of the crust. As melt cools and solidifies, a proportion of this fluid will be released into the crust. Provided permeable pathways allow such fluids to ascend, they can contribute to the advective heat-transfer within the crust.

Model M3 models fluid advection in the simplest form possible, by imposing a flow-rate entering the base of the crust of 0.5 mm yr^{-1} (Figure 4). No account is taken of the complex interplay between water bound in magma and free water at the melt-rock interface, so this model is a rather inaccurate representation of effects of magmatic fluid flux from depth. As for the previous models, we neglect convective cooling by fluid circulation in the brittle crust. We assume Darcy flow with a base permeability in the crust of 10^{-17} m^2 (brittle crust) and 10^{-21} m^2 (ductile crust and melt). Model M3 is otherwise identical to M2 without melt convection.

The advective effects of basal fluid flux push the thermal gradient upwards slightly towards the surface. As a result, surface heat-flow is slightly higher. The increased transfer of heat at depth, however, also causes a greater degree of melting in the lower crust. It is difficult to envision how additional fluid flux would avoid wholesale melting of lower crust while still not being sufficient to generate enough surface heat-flux to match observations.

1.2.4 2D model slice with underplating, rifting, and melt conduit allowing shallow melt in the brittle crust

Model M4 is similar to M2 but a temperature of 900°C is prescribed for a small region of the upper crust representing injection of hot melt along a thin dike from the underplated

region. The dike itself (and mechanism of melt transport) is not modelled. The prescribed thermal anomaly representing melt injection is 2-km-wide, 500m-thick and placed at 7 km depth (Figure 5). As a result, surface heat-flow is increased to ca. 280 mWm^{-2}. With convective fluid transfer in the brittle crust surrounding the shallow intrusion, heat-flux near the surface would be expected to be even higher, since heat-flow peaks at ~ 500 mW m^{-2} just above the shallow melt.

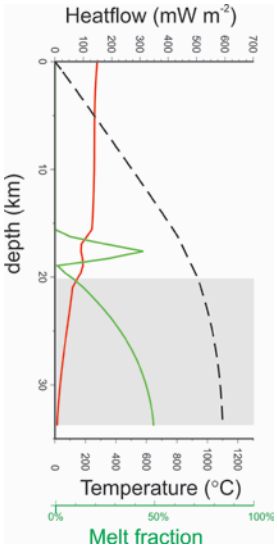

Figure 4: Results for model M3 after 3 My of underplating, stretching and fluid flux (0.5 mm yr^{-1} into the base of the model). (a) (solid lines) no melt convection; (b) (dashed lines) with melt convection for melt fraction > 40%. Black is temperature; red is heat-flow; green shows melt fraction. Grey = underplated, stretched basalt.

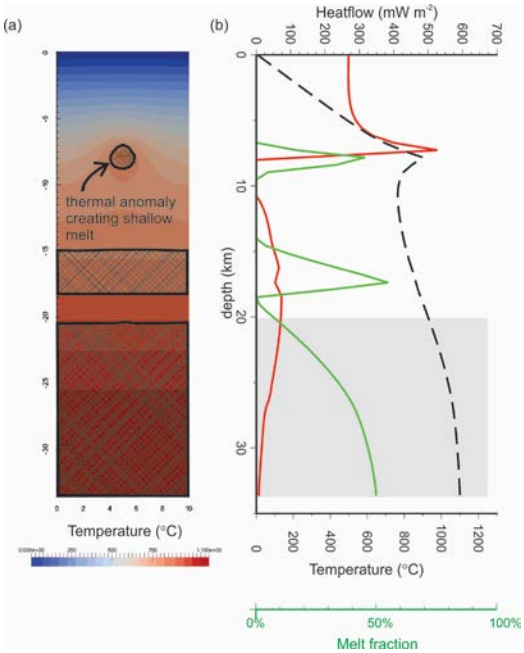

Figure 5: Results for model M4 after 3 My of underplating, stretching and with an thermal anomaly causing partial melting over a small region in the upper crust. (a) 10-km-wide model with no-flow side boundaries. Colour contours are temperature; shaded regions have partial melt fraction > 10%. (b) Profile through the middle of the model. Black dashed line is temperature; red is heat-flow; green shows melt fraction. Grey shading indicates zone of underplated and stretched basalt.

1.2.5 2D model of Taupo rift with underplating, rifting, and shallow melt in the brittle crust

The final thermo-mechanical model M5 is fully two-dimensional and uses some of the boundary conditions discussed in the previous 1D models (Figure 6). The model starts from a uniformly-30km-thick greywacke crust. It is extended at 1 cm yr^{-1}. Basaltic melt is underplated beneath the central 60 km of the model and the temperature there is perturbed from background 480°C to 1100°C representing addition of partial melt from the underlying subduction system. A fluid flux of 0.5 mm yr^{-1} is also added at the base. Other properties are the same as the 1D models.

At the onset of rifting the thermal profile has a uniform gradient of 16 °Ckm^{-1}. A 500m-thick, 2 km-wide layer at 900°C is added at 6 km depth to simulate injection of a mafic melt layer at shallow depths. This causes melting of surrounding greywacke crust. In addition, a small amount of sedimentation of the top surface is applied dependent on local height above base-level. Greywacke crust is given a coefficient of friction of 0.6, softening to 0.09 with brittle strain > 50%. Ductile properties are based on wet quartzite (Gleason and Tullis, 1995). Local isostatic compensation is applied at the base of the model, which is otherwise free to move horizontally.

After 750 kyr the rift has reached a deformation state similar to the present-day Ngakuru graben (Figure 6).

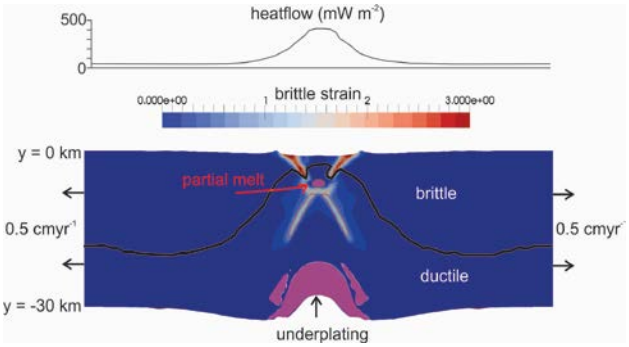

Figure 6: Results for 2D rifting model M5 after 0.75 My of underplating, stretching and with an thermal anomaly causing partial melting. Surface heat flow shown at top. Brittle strains of >200% show faults that have developed above the zone of partial melt. Black line separates brittle and ductile layers, which are determined naturally in the model as a function of ambient strain-rates, temperatures, and pressures. Purple-filled regions have partial melt > 10%. No vertical exaggeration.

Figure 6 shows two inward-dipping faults that have developed above the thermal anomaly caused by underplating and shallow melt. These approximately correspond to the geometry of the Ngakuru and Paeroa faults. The brittle-ductile transition shallows to only a few km deep above the intrusion. Surface heat-flow in this region is over 400 mW m^{-2}. This model demonstrates how a shallow intrusion can substantially alter surface heat-flow around it and cause deformation to focus into a narrow rift.

However, many features in this simple 2D model are unlike the Ngakuru graben. The shallowing of the brittle-ductile transition in the model is not supported by data showing that the base of seismicity in the TVZ is uniformly ~ 6-7 km deep (Bryan et al., 1999; Sherburn et al., 2003). This is partly because model M5 does not include effects of convective heat transport of fluids through brittle crust. Most importantly, the Ngakuru graben has regions of upflow and downflow along permeable faults, with geothermal activity concentrated on the rift's western and eastern margins. To investigate these effects, we require more sophisticated fluid-flow models to investigate the interaction of high heat-flow with fluid-flow in the rift, which is the topic of the next section.

2. FLUID-FLOW MODELS IN THE BRITTLE UPPER CRUST OF THE NGAKURU GRABEN

In this section we present some first-order models of fluid and heat flow within the fault system of the Ngakuru Graben. This builds and improves on the work described in Kissling et al., (2015) by using a new modelling code 'tgns' (Kissling, 2014) which incorporates a new meshing technique which allows resolution of flows at length scales well below that of the fault zone widths (taken here to be 100 m). The aim of the modelling is to explain the presence of recent (< 30 ka) surface flows of hydrothermal fluid from each of the four fault systems within the Ngakuru Graben. To do this, we search for regions of 'permeability space' where the Ngakuru Graben hydrological system is sensitive to small changes in the fault permeabilities (because of rupturing or sealing) which can lead to changes in the location of the surface outflows. Here we present some examples where the permeabilities of the four fault systems are assumed to be the same.

2.1 Model setup and fault architectures

The domain for the fluid flow model is 30 km wide and 7 km deep (only the central ~14 km are shown in Figures 6 and 8). At the top surface of the model we prescribe fully liquid-saturated conditions at 20°C and 10 bars, the pressure being chosen to reduce boiling in the near-surface which can significantly slow the computation. At the lower boundary we apply a Gaussian heat source with a peak heat flow of 700 mWm^{-2} and a half-width of ~ 2 km, located at X = 17.5 km (see Figure 7), just to the east of the central Ngakuru graben and consistent with MT observations interpreting a region of upwelling fluids and/or partial melt to the east of Te Kopia (Bertrand et al., 2012). Initial conditions for the model are hydrostatic pressure corresponding to a vertical temperature gradient of 25°C/km. We use permeabilities of 10^{-15} m^2 for the shallow volcanics (to 2 km depth within the graben and 1 km outside) and 10^{-16} m^2 for the basement rocks interior to the graben (below 2 km).

The model includes the four major fault systems in the Ngakuru graben – from west to east the Ngakuru, Maleme, Whirinaki and Paeroa faults. Villamor and Berryman (2001) give typical fault dips of 75° at the surface for the faults in the Ngakuru graben and propose dips of 60° at seismogenic depths, although they state that this is poorly constrained and that the deep subsurface expression of the faults is unknown. Here we adopt 60° surface dips for all faults, with the Ngakuru and Maleme faults dipping to the southeast and Whirinaki and Paeroa toward the northwest. All faults are assumed to have a uniform permeability and a constant width of 100 m. The Ngakuru, Maleme, Whirinaki and Paeroa faults intersect the surface at X=10 km, 13.5 km, 15.3 km and 21 km respectively. Here we present two models with different architectures at depth:

- Model F1 – all faults are linear and maintain constant dip. The Maleme and Whirinaki faults are terminated where they intersect Paeroa and Ngakuru faults respectively.
- Model F2 – Ngakuru, Maleme and Whirinaki faults are linear, and intersect (and terminate at) the listric Paeroa fault. In this model the dip of the Paeroa fault decreases to ~20° at 6 km depth.

We present some results from these models where the permeabilities of the four fault systems are assumed to be the same. All models are run for a period of 100 kyr until a near-steady state is reached.

2.2 Results

Figure 7 shows a typical temperature distribution for model F1. In this case the permeabilities of all the faults are 100 mD. The figure shows that Paeroa fault hosts an upflow of hot fluid, while downflows of cool surface water occur on Ngakuru and Maleme and upper Whirinaki faults. Note also that a small upflow on the lower Whirinaki fault, below where it intersects the Maleme fault, is cut off the much stronger downflow on that (Maleme) fault. This occurs despite the permeability of both faults being the same.

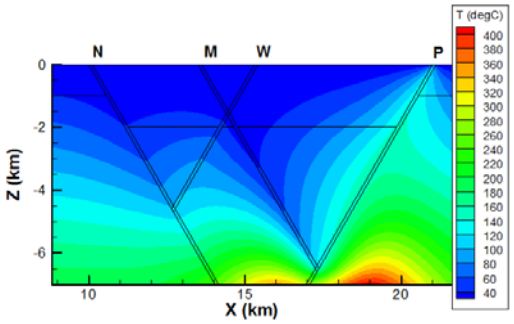

Figure 7: Temperature distribution for model F1 fault architecture with all fault permeabilities equal to 100 mD (10^{-13} m^2). The faults are labelled N, M, W and P for Ngakuru, Maleme, Whirinaki and Paeroa respectively.

This mechanism appears in many models and can result in the surface in/outflows from the faults being very sensitive to small permeability changes. Figure 8 shows how the surface flows associated with each fault change as their (common) permeability changes. Between 100 and 150 mD there is a major change in the character of these flows. Below 100 mD Paeroa fault hosts the only upflow but above 150 mD this changes to a downflow and Whirinaki fault then hosts the only upflow. Over the range of permeabilities shown on the figure Ngakuru and Maleme faults support

weak downflows which switch magnitude in the same 100-150 mD range.

Figure 9 shows a typical result for model F2, again with all the fault permeabilities being 100 mD. In this example, the upflow is hosted by the Whirinaki fault with weak to moderate strength downflows on the other three faults. Note that the surface upflow on the Whirinaki fault actually has its beginnings on the lower Maleme fault where it is appears to be fed almost directly from the heat source. At shallower levels, ~1.5 km depth, the flow is diverted into the upper Whirinaki fault at the intersection with the Maleme fault. As with model A, a major change in flow direction occurs even though all the fault permeabilities are equal. In this case, the diversion of the upflow into the upper Whirinaki fault is presumably caused by the weak downflow in the upper Maleme fault. The sensitivity of this weak downflow to the fault permeabilities is unknown at present, but it seems possible that only a small change in the permeabilities could cause the upflow to reach the surface through the Maleme fault.

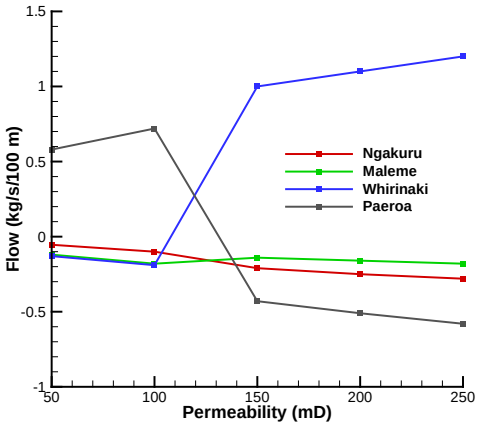

Figure 8: Surface flows for model F1 fault architecture with all fault permeabilities equal. A positive flow indicates an outflow at the surface.

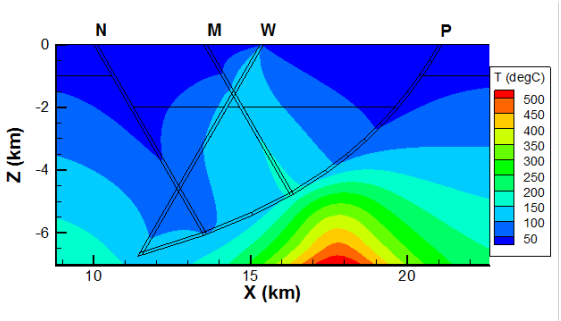

Figure 9: Temperature distribution for model F2 fault architecture with all fault permeabilities equal to 100 mD. The faults are labelled N, M, W and P for Ngakuru, Maleme, Whirinaki and Paeroa respectively.

This conjecture is confirmed by Figure 10, which shows the surface flows for model F2 as a function of the fault permeability. As with model F1 an exchange of flows occurs, but this time between the Maleme and Whirinaki faults. This exchange occurs (coincidentally) between 100 and 150 mD, while weak downflows are maintained in Ngakuru and Paeroa faults over the entire range of permeabilities.

3. CONCLUSIONS

The numerical experiments shown in this paper need careful consideration and improvement to better explore heat transfer in the deep crust below the TVZ. In particular, the thermo-mechanical models in Section 1 neglect the effect of convective heat transfer in brittle crust (e.g., Kissling, 2004; Kissling and Weir, 2005). Convective hot-plate models require steady high heat-flows of >~ 400 mW m^{-2} at the brittle-ductile transition to drive convective flow at shallower depths (Kissling and Weir, 2005). Not surprisingly, the models in Section 1 illustrate that the only way to get sufficient heat flux at mid-crustal levels without wholesale melting of lower crust is by an advective transfer of heat from deeper melt (e.g., Bibby et al., 1995).

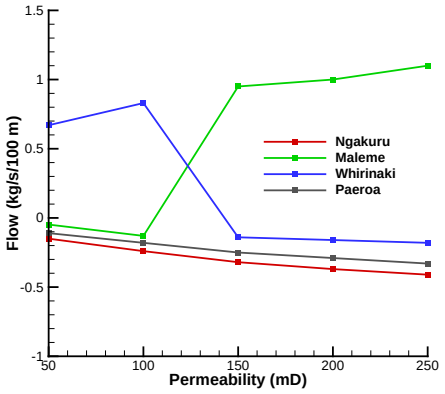

Figure 10: Surface flows for model F2 fault architecture with all fault permeabilities equal. A positive flow indicates an outflow at the surface.

This supports the conclusion that the unusually high heat flux measured at the surface in the TVZ results from the presence of partial melt at shallow depths near the brittle-ductile transition (~ 7 km depth). Although not all geothermal systems may be directly driven by underlying, cooling melt bodies, the overall high heat-flow in the rift depends on them, because the presence of such bodies within the rift helps to thermally insulate lower layers and transfer deep heat to the surface. Other mechanisms to transfer heat from underplated melt at the base of the crust, such as conductive cooling and fluids, would lead to too much melting of deeper greywacke crust, which is inconsistent with volumes of partial melt in the crust derived from MT inversions (Ellis et al., 2015).

Two detailed models of the Ngakuru Graben hydrological system have been developed. We assumed a Gaussian heat source at the brittle-ductile transition representing a cooling intrusive body. Recent MT data indicate that the rift in this region is no longer underlain by shallow partial melt. Bertrand et al. (in press) suggest that the geothermal circulation in this region is fed by a waning magmatic system, where intrusive heat sources have cooled below the solidus and become resistive. Alternatively, deep structure extending through the brittle and ductile crust may play a greater role in focusing hot fluid flow than we have assumed, for example if the Paeroa Fault is obscuring an earlier volcanic structure (e.g., Downs et al., 2014).

The fluid-flow models assume a brittle crust to 7 km depth, but have very different deeper fault architectures. Both models show that fluid flow in a graben setting with intersecting faults is complex, with flow diversions occurring where faults intersect and the location of surface outflows (i.e. surface hydrothermal systems) being highly sensitive to the fault permeabilities. In particular, the two models show that surface outflows can jump to nearby faults when permeabilities lie in certain quite narrow ranges. Changes to fault permeabilities over time from fault evolution, rupturing and/or sealing (e.g., Dempsey et al., 2012, 2013) may also be relevant to the presence of widespread and sporadic fossil hydrothermal deposits in the Ngakuru Graben.

ACKNOWLEDGEMENTS

The thermo/mechanical/fluid code SULEC was developed jointly with Susanne Buiter (NGU). Discussions with Grant Caldwell, Ted Bertrand, Wiebke Heise, and Stephen Bannister are gratefully acknowledged. This work was funded by Core Science Funding to GNS Science though the Geothermal Resources programme.

REFERENCES

Annen, C., Blundy, J.D., Sparks, R.S.: The genesis of intermediate and silicic magmas in deep crustal hot zones, Journal of Petrology (2005).

Bertrand, E.A., Caldwell, T.G., Hill, G.J., Wallin, E.L., Bennie, S.L. Cozens, N., Onacha, S. A., et al.,: Magnetotelluric imaging of upper-crustal convection plumes beneath the Taupo Volcanic Zone, New Zealand. Geophysical Research Letters 39 (2012).

Bertrand, E.A., Caldwell, T.G., Bannister, S., Soengkono, S., Bennie, S.L., Hill, G.J., Heise, W.: Using array MT data to image the crustal resistivity structure of the southeastern Taupo Volcanic Zone, New Zealand. In press (2015).

Bibby, H.M., Caldwell, T.G., Davey, F.J., Webb. T.H.: Geophysical evidence on the structure of the Taupo Volcanic Zone and its hydrothermal circulation. Journal of Volcanology and Geothermal research 68, 29-38 (1995).

Bryan, C.J., Sherburn, S., Bibby, H.M., Bannister, S.C., Hurst, A.W.: Shallow seismicity of the central Taupo Volcanic Zone, New Zealand: Its distribution and nature. New Zealand Journal of Geology and Geophysics, 42, 533–542 (1999).

Dempsey, D.E., Rowland, J.V., Zyvoloski, G.A., Archer, R.A.: Modeling the effects of silica deposition and fault rupture on natural geothermal systems. Journal of Geophysical Research, 117 (2012).

Dempsey, D.E., Archer, R.A., Ellis, S.M., Rowland, J.V.: Hydrological effects of dip-slip fault rupture on a hydrothermal plume. Journal of Geophysical Research: Solid Earth, 118, 195-211 (2013).

Downs, D.T., Wilson, C.J.N., Cole, J.W., Rowland, J.V., Calvert, A.T., Leonard, G.S., Keall, J.M.: Age and eruptive center of the Paeroa Subgroup ignimbrites (Whakamaru Group) within the Taupo Volcanic Zone of New Zealand. Geological Society of America Bulletin 126, 1131-1144 (2014).

Ellis, S., Heise, W., Kissling, W., Villamor, P., Schreurs, G.: The effect of crustal melt on rift dynamics: case study of the Taupo Volcanic Zone. New Zealand Journal of Geology and Geophysics, 57, 453-458 (2014).

Gleason, G.C., Tullis, J.: A flow law for dislocation creep of quartz aggregates determined with the molten salt cell. Tectonophysics, 247, 1-23 (1995).

Harrison, A., White, R.S.: Lithospheric structure of an active backarc basin: the Taupo Volcanic Zone, New Zealand. Geophysical Journal International, 167, 968-990 (2006).

Heise, W., Bibby, H.M., Caldwell, T.G., Bannister, S.C., Ogawa, Y., Takakura, S., Uchida, T.: Melt distribution beneath a young continental rift: the Taupo Volcanic Zone, New Zealand. Geophysical Research Letters, 34 (2007).

Heise, W., Caldwell, T.G., Bibby, H.M., Bennie, S.L.: Three-dimensional electrical resistivity image of magma beneath an active continental rift, Taupo Volcanic Zone, New Zealand. Geophysical Research Letters 37 (2010).

Hochstein, M.P.: Crustal heat transfer in the Taupo Volcanic Zone (New Zealand): comparison with other volcanic arcs and explanatory heat source models. Journal of Volcanology and Geothermal Research, 68, 117-151 (1995).

Kissling, W.M.: Deep hydrology of the geothermal systems in the Taupo Volcanic Zone, New Zealand. *Doctoral dissertation, ResearchSpace@ Auckland* (2004).

Kissling, W.M., Weir, G.J.: The spatial distribution of the geothermal fields in the Taupo Volcanic Zone, New Zealand. Journal of volcanology and geothermal research, 145, 136-150 (2005).

Kissling, W., Rae, A., Villamor, P., Ellis, S.: Hydrothermal Fluid Flow in a Structurally-controlled Basin, Ngakuru Graben, Taupo Rift, New Zealand. *Proc. World Geothermal Congress 2015*, Melbourne, Australia.

Kissling, W.M.: A testbed for a new-generation geothermal simulator. Proc. 36th New Zealand Geothermal Workshop, Auckland, New Zealand. (2014).

Rippe, D., Unsworth, M.: Quantifying crustal flow in Tibet with magnetotelluric data. Physics of the Earth and Planetary Interiors, 179, 107-121 (2010).

Rosenberg, C.L., Handy, M.R.: Experimental deformation of partially melted granite revisited: implications for the continental crust. Journal of metamorphic Geology, 23, 19-28 (2005).

Sibson, R.H., Rowland, J.V.: Stress, fluid pressure and structural permeability in seismogenic crust, North Island, New Zealand. Geophysical Journal International 154, 584-594 (2003).

Stern, T., Stratford, W., Seward, A., Henderson, M., Savage, M., Smith, E., Benson, A., Greve, S., Salmon, M.: Crust–mantle structure of the central North Island, New Zealand, based on seismological observations. Journal of Volcanology and Geothermal Research, 190, 58-74 (2010).

Stratford, W.R., Stern, T.A.: Crust and upper mantle structure of a continental backarc: central North Island, New Zealand. Geophysical Journal International, 166, 469-484 (2006).

Waff, H.S., Weill, D.F.: Electrical conductivity of magmatic liquids: effects of temperature, oxygen fugacity and composition. Earth and Planetary Science Letters, 28, 254-260 (1975)..

Weir, G.J.: Energy transport processes in a brittle–ductile intrusive model of the Taupo Volcanic Zone, New Zealand. Journal of Volcanology and Geothermal research 84 61-72 (1998).